

1 **Impact of grids and dynamical cores in CESM2.2 on**
2 **the meteorology and climate of the Arctic**

3 **Adam R. Herrington** ¹, **Marcus Lofverstrom** ², **Peter H. Lauritzen** ¹ and
4 **Andrew Gettelman** ¹

5 ¹National Center for Atmospheric Research, 1850 Table Mesa Drive, Boulder, Colorado, USA
6 ²Department of Geosciences, University of Arizona, 1040 E. 4th Street, Tucson, AZ USA

7 **Key Points:**

- 8 • enter point 1 here
9 • enter point 2 here
10 • enter point 3 here

Abstract

[enter your Abstract here]

Plain Language Summary

[enter your Plain Language Summary here or delete this section]

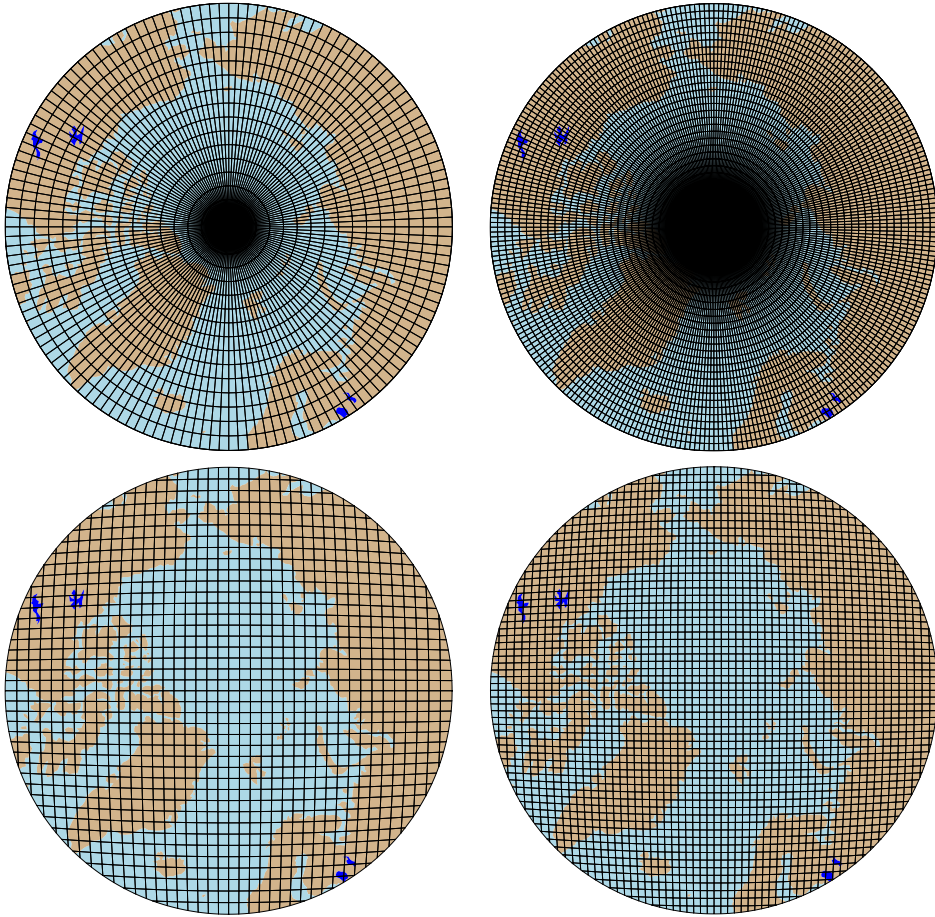
1 Introduction

General Circulation Models (GCMs) are powerful tools for understanding the meteorology and climate of the high-latitudes, which are among the most sensitive regions on Earth to global and environmental change. Despite their importance, the numerical treatment of polar regions is handled in vastly-different ways due to the so-called *pole-problem* (Williamson, 2007). The pole-problem refers to instability arising from the convergence of meridians at the polar points on latitude-longitude grids (e.g., Figure 1a). Depending on the numerics, methods exist to stabilize the pole problem, and latitude-longitude grids may be advantageous for polar processes as structures can be represented with more degrees of freedom than elsewhere in the computational domain. With the recent trend towards globally uniform unstructured grids, any potential benefits of latitude-longitude grids on polar regions may become a relic of the past. In this study, a spectrum of grids and dynamical cores (hereafter referred to as *dycores*) available in the Community Earth System Model, version 2.2 (CESM; <http://www.cesm.ucar.edu/models/cesm2/>), from conventional latitude-longitude grids to unstructured grids with globally uniform grid spacing to unstructured grids with regional refinement over the Arctic, are evaluated to understand their impacts on the simulated characteristics of the Arctic, with a special focus on the Greenland Ice Sheet.

In the 1970's the pole problem was largely defeated through wide-spread adoption of efficient spectral transform methods in GCMs. These methods transform grid point fields into a global, isotropic representation in wave space, where linear operators in the equation set can be solved for exactly. While spectral transform methods are still commonly used in the 21st century, local numerical methods have become desirable for their ability to run efficiently on massively parallel systems. The pole-problem has thus re-emerged in contemporary climate models that use latitude-longitude grids, and some combination of reduced grids and polar filters are necessary to ameliorate this instability (Jablonowski & Williamson, 2011). Polar filters are akin to a band-aid; they subdue the growth of unstable modes by applying additional damping to the solution over polar regions. One might expect that this additional damping reduces the effective resolution such that the resolved scales are similar across the entire domain, but this seems an unlikely and is explored further in this study.

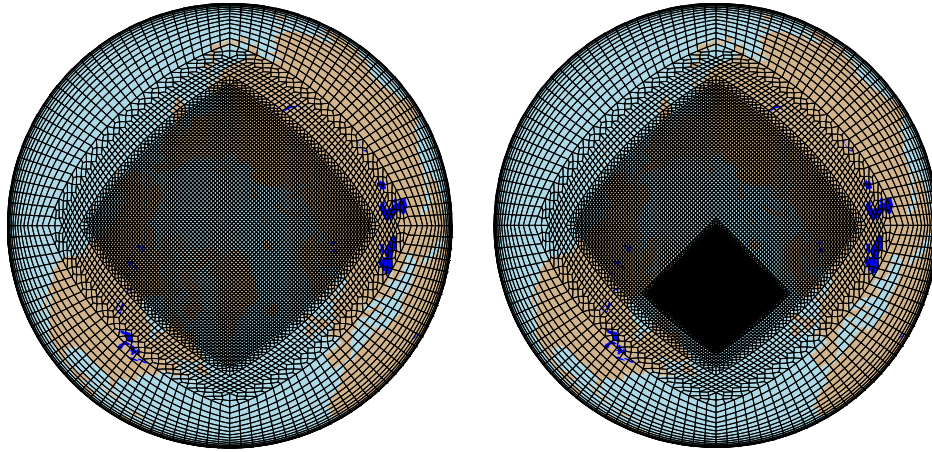
An alternative approach is to use unstructured grids. Unstructured grids allow for more flexible grid structures, permitting quasi-uniform grid spacing globally that eliminates the pole-problem entirely (e.g., Figure 1c). This grid flexibility also allows for variable-resolution or regional grid refinement. Grids can be developed with refinement over polar regions that could in principle make up for any loss in polar resolution in transitioning away from latitude-longitude grids (e.g., Figure 2), although this comes at the cost of a smaller CFL-limiting time-step in the refined region. But unstructured grids scale more efficiently on parallel systems than latitude-longitude grids, resulting in latitude-longitude grids becoming less common, and unstructured grids more common as computing power continued to increase over time.

The meteorology and climate of the Arctic is characterized by a range of processes and scales that are difficult to represent in GCMs (Bromwich et al., 2001; Smirnova & Golubkin, 2017; van Kampenhout et al., 2018). Synoptic scale storms are well represented

**Figure 1.** .

59 at typical GCM resolutions, but mesoscale Polar Lows are not. These mesoscale systems
 60 are prevalent during the cold season, and produce gale-force winds that can induce large
 61 fluxes through the underlying sea-ice/ocean interface. The Arctic also contains the Green-
 62 land Ice Sheet (hereafter denoted as *GrIS*). While it blankets the largest island in the
 63 world (Greenland), *GrIS* is only marginally resolved at typical GCM resolutions. *GrIS*
 64 ablation zones exert a primary control on the mass balance of the ice sheet, but are on
 65 the order of 100km wide, and models struggle to resolve these narrow features. *GrIS* el-
 66 evations descends rapidly toward the coasts, resulting in steep margins that facilitate oro-
 67 graphic precipitation events, but which are not well resolved in GCMs. The Arctic is there-
 68 fore well-suited to understand the impact of different grids and dycores on processes that
 69 are marginally resolved at conventional GCM resolutions.

70 The goal of this study is to characterize the representation of high-latitude regions
 71 using the spectral-element and finite-volume dycores in CESM2.2, as these models treat
 72 the high-latitudes, e.g., the pole-problem, in very different ways. The manuscript is laid
 73 out as follows. Section 2 consists of documentation of the grids, dycores and physical pa-
 74 rameterizations used in this study. The Arctic refined grids were developed by the au-
 75 thors, and this section serves as their official documentation in CESM2.2. Section 2 also
 76 contains a description of the experiments along with the observational datasets and post-
 77 processing software used for evaluating the models. Section 3 contains the results of the
 78 experiments and Section 4 provides some discussion and conclusions.

**Figure 2.**

2 Methods

2.1 Dynamical cores

The atmospheric component of CESM2.2, the Community Atmosphere Model, version 6.3 (CAM; <https://ncar.github.io/CAM/doc/build/html/index.html>), supports a diverse number of atmospheric dynamical cores. These range from dycores using latitude-longitude grids, the finite-volume (FV; Lin, 2004) and eulerian spectral transform (EUL; Collins et al., 2006) models, and dycores built on unstructured grids, the spectral-element (SE; Lauritzen et al., 2018) and finite-volume 3 (FV3; Putman & Lin, 2007) models. The EUL dycore is the oldest dycore in CAM, and the least supported of all the dycores in the current model. FV3 is the newest dycore in CAM, but it was not fully incorporated at the time this work commenced, and so is omitted from this study. The authors instead focus on the two most well supported dycores in CAM, SE and FV.

2.1.1 Finite-volume dynamical core

The FV dycore is a hydrostatic model that integrates the equations of motion using a finite-volume discretization on a spherical latitude-longitude grid (Lin & Rood, 1997). The 2D dynamics evolve in floating Lagrangian layers that are periodically mapped to Eulerian reference grid in the vertical (Lin, 2004), using a hybrid-pressure vertical coordinate. Hyperviscous damping is applied to the divergent modes while Laplacian damping is applied to momentum in the top few layers, referred to as a *sponge layer* (Lauritzen et al., 2011). A polar filter is used to avoid computational instability due to the convergence of the meridians, allowing for a more practical time-step. It takes the form of a Fourier filter in the zonal direction, with the damping coefficients increasing monotonically poleward (Suarez & Takacs, 1995).

2.1.2 Spectral-element dynamical core

The SE dycore is a hydrostatic model that integrates the equations of motion using a high-order continuous Galerkin method (Taylor et al., 1997; Dennis et al., 2012). The computational domain is a cubed-sphere grid tiled with quadrilateral elements (e.g., Figure 2). Each element contains a fourth order basis set in the two horizontal directions, with the solution defined at the roots of the basis functions, the Gauss-Lobatto-Legendre (GLL) quadrature points. This results in 16 GLL nodal points within each element, with

109 12 of the points lying on the (shared) element boundary. Communication between el-
 110 ements happens via the direct stiffness summation (Canuto et al., 2007), which applies
 111 a numerical flux to the element boundaries that reconciles overlapping nodal point val-
 112 ues and produces a continuous global basis set.

113 As with the FV dycore, the dynamics evolve in floating Lagrangian layers that are
 114 subsequently mapped to a Eulerian reference grid. A dry mass vertical coordinate was
 115 more recently implemented for thermodynamic consistency with condensates (Lauritzen
 116 et al., 2018). The 2D dynamics have no implicit dissipation and so hyperviscosity op-
 117 erators are applied to all prognostic variables to remove spurious numerical errors (Dennis
 118 et al., 2012). Laplacian damping is applied in the sponge layer.

119 The SE dycore supports regional grid refinement via its variable-resolution config-
 120 uration, requiring two enhancements over uniform resolution grids. (1) As the numer-
 121 ical viscosity increases with resolution, explicit hyperviscosity relaxes according to the
 122 local element size, reducing in strength by about an order of magnitude per halving of
 123 the grid spacing. A tensor-hyperviscosity formulation is used (Guba et al., 2014), which
 124 adjusts the coefficients in two orthogonal directions to more accurately target highly dis-
 125 torted quadrilateral elements. (2) The topography boundary conditions need to be smoothed
 126 in a way that does not excite grid scale modes, and so the NCAR topography software
 127 (Lauritzen et al., 2015) was modified to scale the smoothing radius by the local element
 128 size.

129 For spectral-element grids with quasi-uniform grid spacing, a variant in which tracer
 130 advection is computed using the Conservative Semi-Lagrangian Mult-tracer tranport
 131 scheme is used instead (CSLAM; Lauritzen et al., 2017). CSLAM has improved tracer
 132 property preservation and accelerated multi-tracer transport. It uses a seperate grid from
 133 the spectral-element dynamics, through dividing each element into 3×3 quasi-equal area
 134 control volumes. The physical parameterizations are computed from the state on the CSLAM
 135 grid, which has clear advantages over the default SE dycore in which the physics are eval-
 136 uated at the GLL nodal points (A. Herrington et al., 2018).

137 2.2 Grids

138 Six grid are evaluated in this study (Table X). The FV dycore is run with 1° and
 139 2° grid spacing, referred to as $f09$ and $f19$, respectively (Figure 1a,b). The 1° equiv-
 140 alent of the CAM-SE-CSLAM grid is also run, referred to as $ne30pg3$ (Figure 1c), where
 141 ne refers to a grid with of $ne \times ne$ elements per cubed-sphere face, and pg denotes that
 142 there are $pg \times pg$ control volumes per element for computing the physics. An additional
 143 1° CAM-SE-CSLAM grid is run, but with the physical paramerizations computed on a
 144 grid that contains 2×2 control volumes per element, $ne30pg2$ (Figure 1d; A. R. Her-
 145 rington et al., 2019).

146 Two variable resolution meshes were developed as part of the CESM2.2 release that
 147 contains grid refinement over the Arctic (Figure 2). The Arctic meshes were developed
 148 using the software package SQuadgen (<https://github.com/ClimateGlobalChange/squadgen>). The *ARCTIC* grid is a 1° grid with $\frac{1}{4}^\circ$ regional refinement over the broader
 149 Arctic region. The *ARCTICGRIS* grid is identical to the *ARCTIC* grid, but contains
 150 an additional patch covering the big island of Greenland with $\frac{1}{8}^\circ$ resolution.

152 2.3 Physical parameterizations

153 The CAM6 physical parameterization package (hereafter referred to as the *physics*;
 154 <https://ncar.github.io/CAM/doc/build/html/index.html>) is used for all simula-
 155 tions in this study. CAM6 physics is most noteably different from it's predecessors through
 156 the incorporation of high-order turbulence closure, Cloud Layers Unified by Binormals
 157 (CLUBB; Golaz et al., 2002; Bogenschutz et al., 2013), which jointly acts as a PBL, shal-

158 low convection and cloud macrophysics scheme. CLUBB is coupled with the MG2 microphysics scheme (Gettelman et al., 2015), with prognostic precipitation and classical
 159 nucleation theory in representing cloud ice for improved cloud-aerosol interactions. Deep
 160 convection is parameterized using a convective quasi-equilibrium mass flux scheme (Zhang
 161 & McFarlane, 1995; Neale et al., 2008) including convective momentum transport (Richter
 162 et al., 2010). PBL form drag is modeled after (Beljaars et al., 2004) and orographic grav-
 163 ity wave drag is represented with an anisotropic method informed by the orientation of
 164 topographic ridges at the sub-grid scale.

166 The CAM convention is that the physics package determines the vertical resolu-
 167 tion. Since all runs use CAM6 physics, all grids and dycores use 32 levels in the verti-
 168 cal, with a model top of about 1 hPa or about 40 km. The physics time-step, in con-
 169 trast, is dependent on grid resolution. Increases in horizontal resolution permit faster
 170 vertical velocities that reduce characteristic time-scales, and so the physics time-step should
 171 be reduced to avoid large time truncation errors (A. Herrington & Reed, 2018). The *ARCTIC*
 172 and *ARCTICGRIS* grids are therefore run with a 4× and 8× reduction in physics time-
 173 step relative to the default 1800 s time-step used in coarser, uniform resolution grids.

174 2.4 Experimental design

175 All grids and dycores are run using an identical transient 1979-1998 AMIP-style
 176 configuration, with prescribed monthly SST/sea-ice after (Hurrell et al., 2008). This con-
 177 figuration refers to the *FHIST compset* and runs out of the box in CESM2.2. The Com-
 178 munity Land Model (CLM5; https://escomp.github.io/ctsm-docs/versions/release-clm5.0/html/users_guide/index.html), which uses the same grid as the atmosphere
 179 grid, calculates the surface energy balance at each land tile within a grid cell, which is
 180 used to compute snow and bare ice melting to inform the surface mass balance (SMB)
 181 of a glacier unit (van Kampenhout et al., 2020). Ice accumulation is modeled as a cap-
 182 ping flux, or snow in excess of the assumed 10 m snow cap, and refreezing of liquid within
 183 the snowpack additionally acts as a source of mass in the SMB calculation. Since the
 184 10 m snowcap needs to be reached in the accumulation zone to simulate the SMB, the
 185 snow depths in the variable-resolution grids were spun-up by forcing CLM5 offline, cy-
 186 cling over 20 years of a fully coupled *ARCTIC* run for about 500 years. The uniform
 187 resolution grids are all initialized with an SMB from an existing *f09* spun-up initial con-
 188 dition.

190 3 Results

191 3.1 Tropospheric temperatures

192 Before delving into the simulated characteristics of the Arctic, an understanding
 193 of the global mean differences between the grids and dycores are assessed, Figure 3 shows
 194 the climatological, zonal mean height plots expressed as differences between the uniform
 195 resolution grids and dycores. The *f09* grid is warmer than the *f19* grid, primarily in the
 196 mid-to-high latitudes and throughout the depth of the troposphere. This is a common
 197 response to increasing horizontal resolution in GCMs (Pope & Stratton, 2002; Roeck-
 198 ner et al., 2006), and (A. R. Herrington & Reed, 2020) has shown that this occurs in CAM
 199 due to greater resolved vertical velocities that in turn, facilitate greater condensational
 200 heating in the macrophyics routine in CLUBB. The right columns in Figure 3 supports
 201 this interpretation, which shows an increase in the climatological CLUBB heating in the
 202 mid-latitudes in the *f09* grid.

203 As the SE dycore is less diffusive than the FV dycore, the resolved vertical veloc-
 204 ities are larger in the SE dycore, and so a modest, resolution-like sensitivity occurs in
 205 which *ne30pg3* is warmer than *f09* (Figure 3). The stratosphere has a different response,
 206 in which *ne30pg3* is much cooler than *f09* in the mid-to-high latitudes. The differences

207 in temperature between *ne30pg3* and *ne30pg2* are small, with a slight warming near the
 208 tropopause at high latitudes. This is consistent with the similar climates found between
 209 these grids in (A. R. Herrington et al., 2019).

210 In comparing the variable-resolution grids to the uniform resolution grids is con-
 211 voluted because not only is the resolution higher in refinement region, but the physics
 212 time-step is shorter in the variable-resolution runs. An additional *ne30pg3* simulations
 213 was run with physics time-step used in the *ARCTIC* grid, referred to as *ne30pg3**. Fig-
 214 ure 4 shows the changes in climatological temperature in zonal-mean height space be-
 215 tween *ne30pg3** and *ne30pg3*. A similar warming response to increase resolution occurs
 216 when the time-step is reduced, and the mechanism is similar in that this facilitates greater
 217 condensational heating by CLUBB. Figure 4 shows difference in climatolgical temper-
 218 ature between the *ARCTIC* grid and the *ne30pg3** grid. The greater condensational heat-
 219 ing and warmer temperatures are confined to the regionally refined region when the im-
 220 pact of physics time-steps is removed from the analysis.

221 3.2 Inter-annual variability

222 3.3 Synoptic-scale storm characteristics

223 3.4 Orographic gravity waves emanating from Greenland

224 3.5 Katabatic winds emanating from Greenland

225 3.6 Greenland surface mass balance

226 4 Conclusions

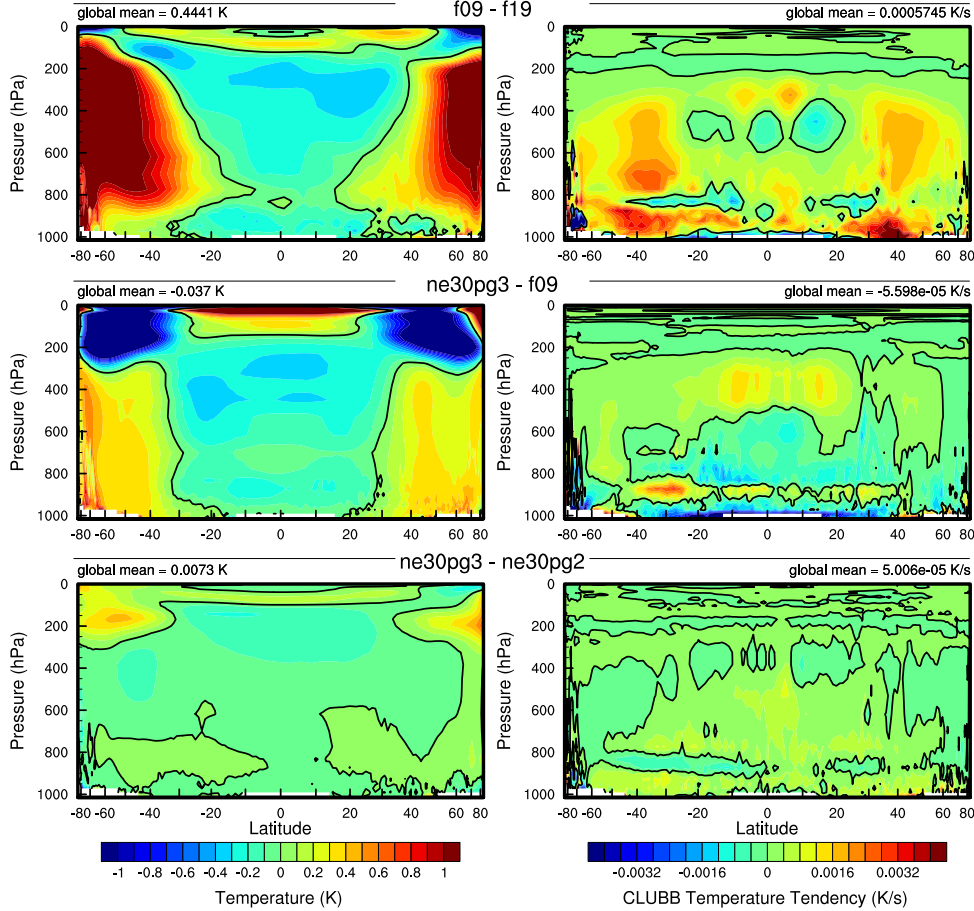
227 Acknowledgments

228 This material is based upon work supported by the National Center for Atmospheric Re-
 229 search (NCAR), which is a major facility sponsored by the NSF under Cooperative Agree-
 230 ment 1852977. Computing and data storage resources, including the Cheyenne super-
 231 computer (doi:10.5065/D6RX99HX), were provided by the Computational and Informa-
 232 tion Systems Laboratory (CISL) at NCAR.

233 The data presented in this manuscript is available at <https://github.com/adamrher/2020-arcticgrids>.

235 References

- 236 Beljaars, A., Brown, A., & Wood, N. (2004). A new parametrization of turbulent
 237 orographic form drag. *Quart. J. Roy. Meteor. Soc.*, *130*(599), 1327–1347. doi:
 238 10.1256/qj.03.73
- 239 Bogenschutz, P. A., Gettelman, A., Morrison, H., Larson, V. E., Craig, C., & Scha-
 240 nen, D. P. (2013). Higher-order turbulence closure and its impact on climate
 241 simulations in the community atmosphere model. *Journal of Climate*, *26*(23),
 242 9655–9676.
- 243 Bromwich, D. H., Cassano, J. J., Klein, T., Heinemann, G., Hines, K. M., Steffen,
 244 K., & Box, J. E. (2001). Mesoscale modeling of katabatic winds over greenland
 245 with the polar mm5. *Monthly Weather Review*, *129*(9), 2290–2309.
- 246 Canuto, C., Hussaini, M. Y., Quarteroni, A., & Zang, T. (2007). *Spectral methods:*
 247 *Evolution to complex geometries and applications to fluid dynamics* (1st ed.).
 248 Springer.
- 249 Collins, W. D., Rasch, P. J., Boville, B. A., Hack, J. J., McCaa, J. R., Williamson,
 250 D. L., ... Zhang, M. (2006). The formulation and atmospheric simulation
 251 of the community atmosphere model version 3 (cam3). *Journal of Climate*,

**Figure 3.**

252

19(11), 2144–2161.

253

Dennis, J. M., Edwards, J., Evans, K. J., Guba, O., Lauritzen, P. H., Mirin, A. A., ... Worley, P. H. (2012). CAM-SE: A scalable spectral element dynamical core for the Community Atmosphere Model. *Int. J. High. Perform. C.*, 26(1), 74–89. Retrieved from <http://hpc.sagepub.com/content/26/1/74.abstract> doi: 10.1177/1094342011428142

257

Gettelman, A., Morrison, H., Santos, S., Bogenschutz, P., & Caldwell, P. (2015). Advanced two-moment bulk microphysics for global models. part ii: Global model solutions and aerosol–cloud interactions. *Journal of Climate*, 28(3), 1288–1307.

261

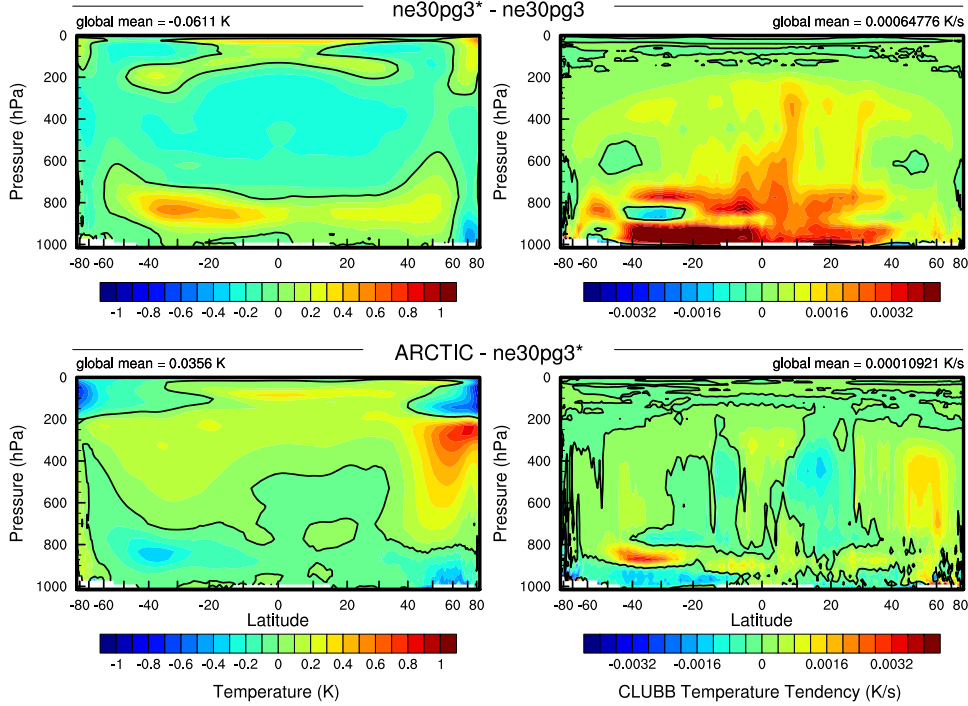
Golaz, J.-C., Larson, V. E., & Cotton, W. R. (2002). A pdf-based model for boundary layer clouds. part i: Method and model description. *Journal of the Atmospheric Sciences*, 59(24), 3540–3551. doi: 10.1175/1520-0469(2002)059<3540:apbmfb>2.0.co;2

266

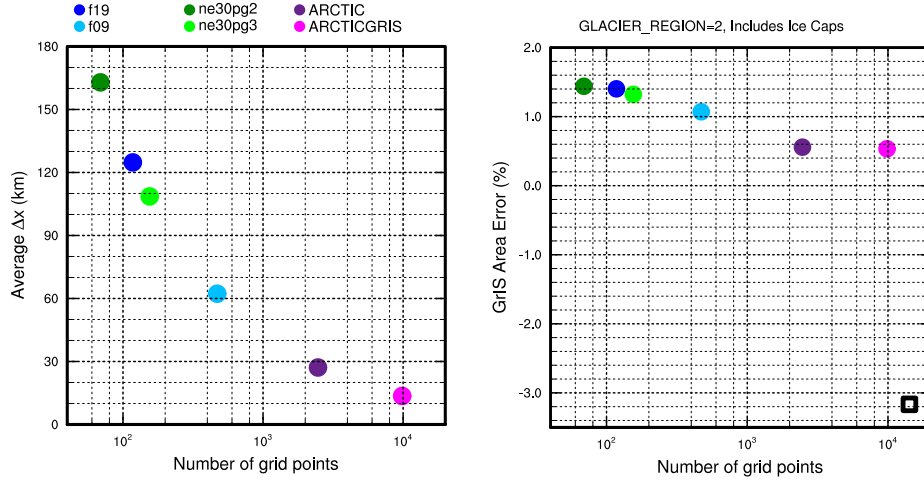
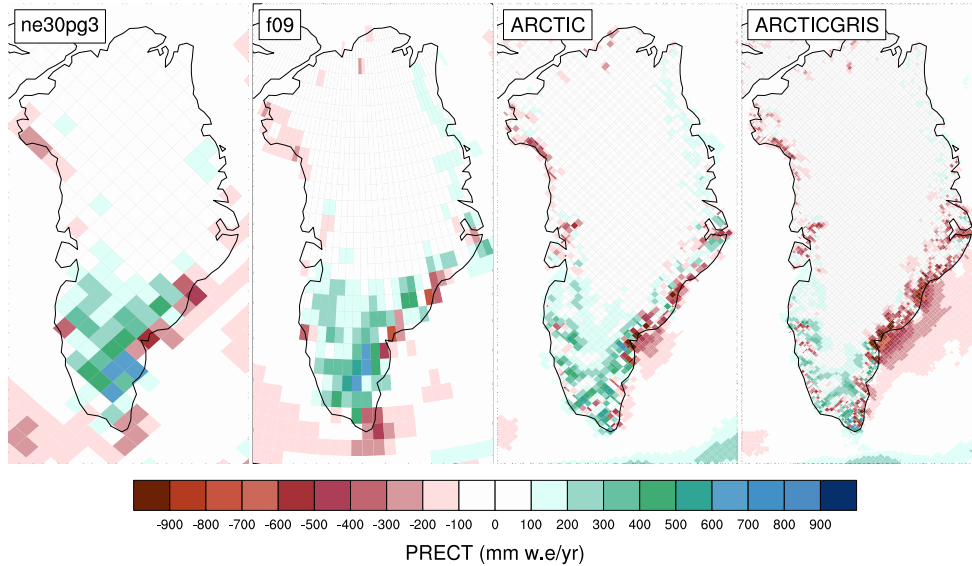
Guba, O., Taylor, M. A., Ullrich, P. A., Overfelt, J. R., & Levy, M. N. (2014). The spectral element method (sem) on variable-resolution grids: evaluating grid sensitivity and resolution-aware numerical viscosity. *Geosci. Model Dev.*, 7(6), 2803–2816. doi: 10.5194/gmd-7-2803-2014

270

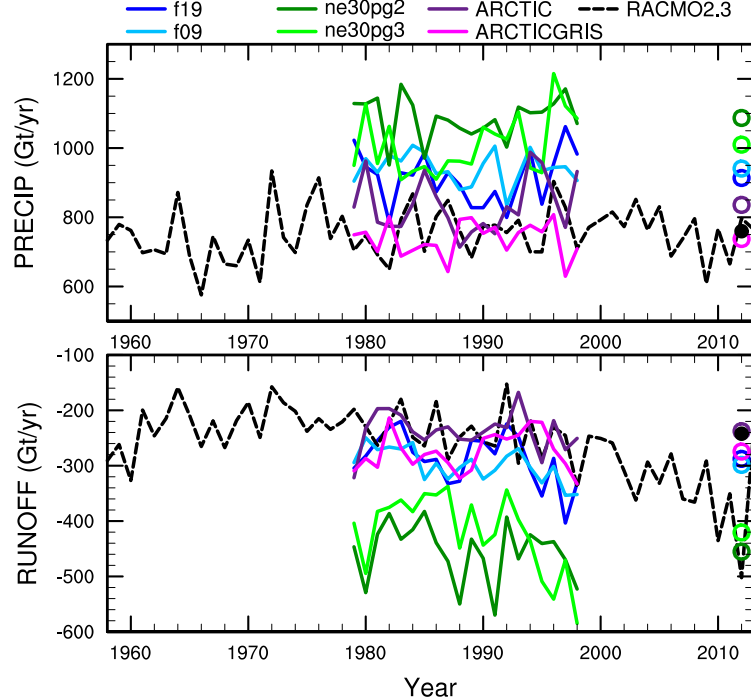
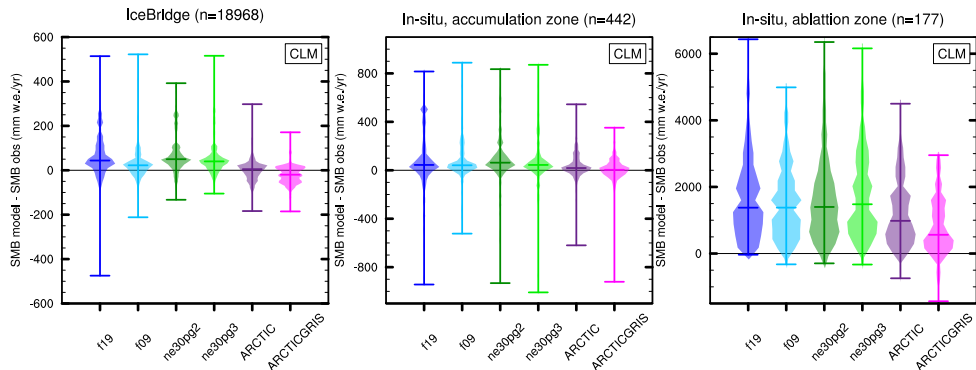
Herrington, A., Lauritzen, P., Taylor, M. A., Goldhaber, S., Eaton, B. E., Bacmeister, J., ... Ullrich, P. (2018). Physics-dynamics coupling with element-based high-order galerkin methods: quasi equal-area physics grid. *Mon. Wea. Rev.*,

**Figure 4.**

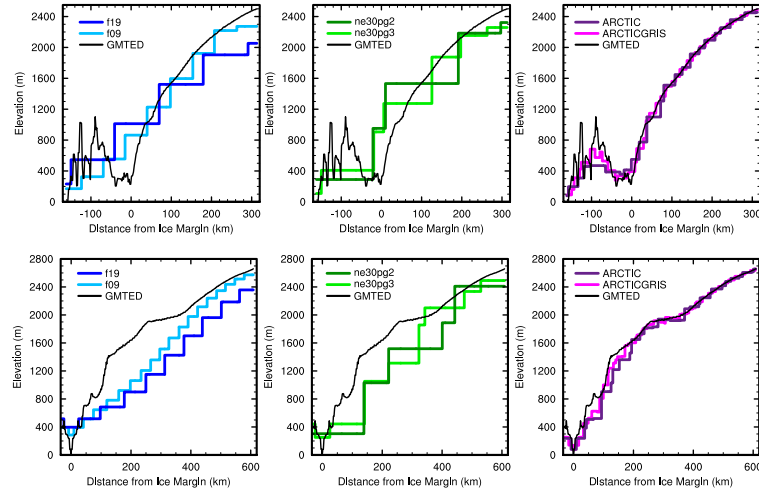
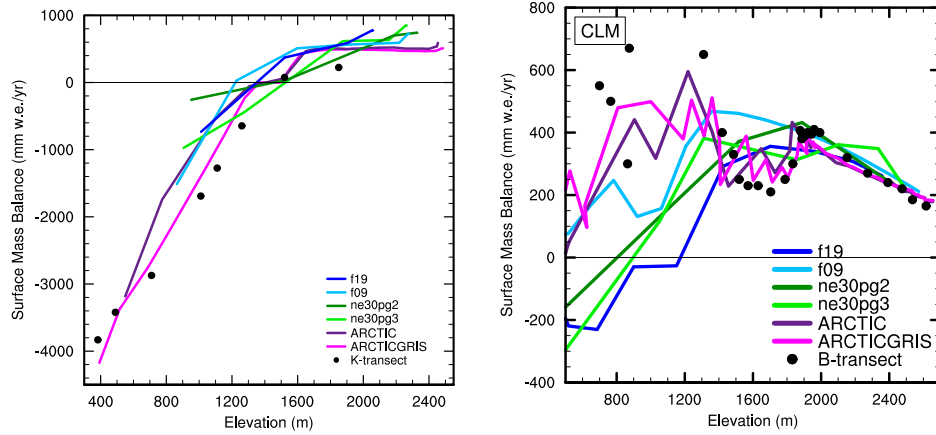
- 273 47, 69–84. doi: 10.1175/MWR-D-18-0136.1
- 274 Herrington, A., & Reed, K. (2018). An idealized test of the response of the commu-
- 275 nity atmosphere model to near-grid-scale forcing across hydrostatic resolutions.
- 276 *J. Adv. Model. Earth Syst.*, 10(2), 560–575.
- 277 Herrington, A. R., Lauritzen, P. H., Reed, K. A., Goldhaber, S., & Eaton, B. E.
- 278 (2019). Exploring a lower resolution physics grid in cam-se-cslam. *Journal of*
- 279 *Advances in Modeling Earth Systems*, 11.
- 280 Herrington, A. R., & Reed, K. A. (2020). On resolution sensitivity in the commu-
- 281 nity atmosphere model. *Quarterly Journal of the Royal Meteorological Society*,
- 282 146(733), 3789–3807.
- 283 Hurrell, J. W., Hack, J. J., Shea, D., Caron, J. M., & Rosinski, J. (2008). A new
- 284 sea surface temperature and sea ice boundary dataset for the community at-
- 285 mosphere model. *Journal of Climate*, 21(19), 5145–5153.
- 286 Jablonowski, C., & Williamson, D. L. (2011). The pros and cons of diffusion, fil-
- 287 ters and fixers in atmospheric general circulation models., in: P.H. Lauritzen,
- 288 R.D. Nair, C. Jablonowski, M. Taylor (Eds.), Numerical techniques for global
- 289 atmospheric models. *Lecture Notes in Computational Science and Engineering*,
- 290 Springer, 80.
- 291 Lauritzen, P. H., Bacmeister, J. T., Callaghan, P. F., & Taylor, M. A. (2015). Ncar
- 292 global model topography generation software for unstructured grids. *Geosci-*
- 293 *entific Model Development Discussions*, 8(6), 4623–4651. doi: 10.5194/gmdd-8
- 294 –4623–2015
- 295 Lauritzen, P. H., Mirin, A., Truesdale, J., Raeder, K., Anderson, J., Bacmeister, J.,
- 296 & Neale, R. B. (2011). Implementation of new diffusion/filtering operators
- 297 in the CAM-FV dynamical core. *Int. J. High Perform. Comput. Appl.*. doi:
- 298 10.1177/1094342011410088
- 299 Lauritzen, P. H., Nair, R., Herrington, A., Callaghan, P., Goldhaber, S., Dennis, J.,

**Figure 5.** .**ANN Climo (1979-1998) minus RACMO ANN Climo (1979-1998)****Figure 6.** .

- 300 ... Dubos, T. (2018). NCAR CESM2.0 release of CAM-SE: A reformulation
301 of the spectral-element dynamical core in dry-mass vertical coordinates with
302 comprehensive treatment of condensates and energy. *J. Adv. Model. Earth
303 Syst.*. doi: 10.1029/2017MS001257
- 304 Lauritzen, P. H., Taylor, M. A., Overfelt, J., Ullrich, P. A., Nair, R. D., Goldhaber,
305 S., & Kelly, R. (2017). CAM-SE-CSLAM: Consistent coupling of a conser-
306 vative semi-lagrangian finite-volume method with spectral element dynamics.
307 *Mon. Wea. Rev.*, 145(3), 833-855. doi: 10.1175/MWR-D-16-0258.1
- 308 Lin, S.-J. (2004). A 'vertically Lagrangian' finite-volume dynamical core for global
309 models. *Mon. Wea. Rev.*, 132, 2293-2307.
- 310 Lin, S.-J., & Rood, R. B. (1997). An explicit flux-form semi-Lagrangian shallow-
311 water model on the sphere. *Q.J.R.Meteorol.Soc.*, 123, 2477-2498.

**Figure 7.****Figure 8.**

- 312 Neale, R. B., Richter, J. H., & Jochum, M. (2008). The impact of convection on
 313 ENSO: From a delayed oscillator to a series of events. *J. Climate*, 21, 5904-
 314 5924.
 315 Pope, V., & Stratton, R. (2002). The processes governing horizontal resolution sensi-
 316 tivity in a climate model. *Climate Dynamics*, 19(3-4), 211–236.
 317 Putman, W. M., & Lin, S.-J. (2007). Finite-volume transport on various cubed-
 318 sphere grids. *J. Comput. Phys.*, 227(1), 55-78.
 319 Richter, J. H., Sassi, F., & Garcia, R. R. (2010). Toward a physically based gravity
 320 wave source parameterization in a general circulation model. *J. Atmos. Sci.*,
 321 67, 136-156. doi: dx.doi.org/10.1175/2009JAS3112.1
 322 Roeckner, E., Brokopf, R., Esch, M., Giorgi, M., Hagemann, S., Kornblueh, L.,
 323 ... Schulzweida, U. (2006). Sensitivity of simulated climate to horizontal

**Figure 9.** .**Figure 10.** .

- 324 and vertical resolution in the echam5 atmosphere model. *Journal of Climate*,
 325 19(16), 3771–3791.
- 326 Smirnova, J., & Golubkin, P. (2017). Comparing polar lows in atmospheric reanal-
 327 yses: Arctic system reanalysis versus era-interim. *Monthly Weather Review*,
 328 145(6), 2375–2383.
- 329 Suarez, M. J., & Takacs, L. L. (1995). Volume 5 documentation of the aries/geos dy-
 330 namical core: Version 2.
- 331 Taylor, M. A., Tribbia, J., & Iskandarani, M. (1997). The spectral element method
 332 for the shallow water equations on the sphere. *J. Comput. Phys.*, 130, 92-108.
- 333 van Kampenhout, L., Lenaerts, J. T., Lipscomb, W. H., Lhermitte, S., Noël, B.,
 334 Vizcaíno, M., ... van den Broeke, M. R. (2020). Present-day greenland ice
 335 sheet climate and surface mass balance in cesm2. *Journal of Geophysical
 336 Research: Earth Surface*, 125(2), e2019JF005318.
- 337 van Kampenhout, L., Rhoades, A. M., Herrington, A. R., Zarzycki, C. M., Lenaerts,
 338 J. T. M., Sacks, W. J., & van den Broeke, M. R. (2018). Regional grid refine-
 339 ment in an earth system model: Impacts on the simulated greenland surface
 340 mass balance. *The Cryosphere Discuss..* doi: 10.5194/tc-2018-257

- 341 Williamson, D. (2007). The evolution of dynamical cores for global atmospheric
342 models. *J. Meteor. Soc. Japan*, 85, 241-269.
- 343 Zhang, G., & McFarlane, N. (1995). Sensitivity of climate simulations to the pa-
344 rameterization of cumulus convection in the canadian climate centre general
345 circulation model. *Atmosphere-ocean*, 33(3), 407-446.